

Premature translation termination mediated non-ER stress induced ATF6 activation by a ligand-dependent ribosomal frameshifting circuit

Hsiu-Ting Hsu¹, Asako Murata², Chikara Dohno², Kazuhiko Nakatani² and KungYao Chang^{1,*}

¹Graduate Institute of Biochemistry, National Chung-Hsing University, Taichung 402, Taiwan and ²SANKEN (The Institute of Scientific and Industrial Research), Osaka University, Mihogaoka 8-1, Ibaraki, Osaka 567-0047, Japan

Received July 19, 2021; Revised March 29, 2022; Editorial Decision March 31, 2022; Accepted April 29, 2022

ABSTRACT

The -1 programmed ribosomal frameshifting (-1 PRF) has been explored as a gene regulatory circuit for synthetic biology applications. The -1 PRF usually uses an RNA pseudoknot structure as the frameshifting stimulator. Finding a ligand-responsive pseudoknot with efficient -1 PRF activity is time consuming and is becoming a bottleneck for its development. Inserting a guanine to guanine (GG)–mismatch pair in the 5'-stem of a small frameshifting pseudoknot could attenuate -1 PRF activity by reducing stem stability. Thus, a ligand-responsive frameshifting pseudoknot can be built using GG-mismatch–targeting small molecules to restore stem stability. Here, a pseudoknot requiring stem–loop tertiary interactions for potent frameshifting activity was used as the engineering template. This considerably amplified the effect of mismatch destabilization, and led to creation of a mammalian -1 PRF riboswitch module capable of mediating premature translation termination as a synthetic regulatory mode. Application of the synthetic circuit allowed ligand-dependent ATF6N mimic formation for the activation of protein folding–related genes involved in the unfolded protein response without an ER-stress inducing agent. With the availability of mismatch-targeting molecules, the tailored module thus paves the way for various mismatch plug-ins to streamline highly efficient orthogonal ligand-dependent -1 PRF stimulator development in the synthetic biology toolbox.

INTRODUCTION

Synthetic biology has been used to solve complicated problems, such as those related to biofuel production and

food shortage, and treat complex diseases including immunotherapeutic applications for cancer (1–3). A main theme in synthetic biology is the development of regulatory gene expression circuits that perform specific functions in a timely manner. Because the advantage of an approach can be specific to a particular problem, diversifying available regulatory modes with as many circuits as possible in the toolbox is crucial. In addition to transcriptional control, posttranscriptional regulation involving RNAs has attracted considerable interest because of its rapid response in protein synthesis regulation (4). RNA circuits capable of directly regulating translation can respond to stimuli without delay for transcription and mRNA export stages in mammalian systems. Because the regulation of translation initiation is frequently observed in nature, it has been the most widely adopted for synthetic purposes (5–7). By contrast, the regulation of translation elongation is less addressed and used.

Programmed -1 ribosomal frameshifting (-1 PRF) occurs during translational elongation and is used by various viruses and bacteria to synthesize two or more proteins at a fixed ratio starting at a single translation initiation site (8,9). Efficient eukaryotic -1 PRF requires two *cis* RNA elements: a hepta nucleotide slippery sequence of X XXY YYZ, where the frameshifting occurs, and a downstream stimulator RNA structure located 5–7 nucleotides (a spacer) away from the slippery sequence. In the slippery sequence, X can be any of the three identical nucleotides, whereas Y represents A or U, and Z represents A, U or C (10). The most commonly observed downstream RNA stimulator is an H-type RNA pseudoknot in which nucleotides from the loop of a stem–loop hairpin form continuing base pairs with a single-stranded region downstream of the hairpin (11). However, not all RNA pseudoknots can stimulate -1 PRF. It has been suggested that a -1 PRF stimulating pseudoknot might act as a roadblock to resist duplex-unwinding activity of an elongating ribosome and thus perturb its reading frame maintenance to facilitate -1 frameshifting at the slippery sequence (from XXY YYZ to

*To whom correspondence should be addressed. Tel: +886 4 22840468 218; Fax: +884 4 22853487; Email: kychang@dragon.nchu.edu.tw

XXX YYY) (12,13). In response to the -1 PRF signal in the mRNA template, some ribosomes are induced to slide one nucleotide backward and then continue translation in the -1 reading frame until reaching a stop codon in the new reading frame. Thus, -1 PRF can either lead to the formation of an extended C-terminal domain or the premature termination of translation depending on the relative positions of the -1 -frame and 0-frame stop codons. In either case, the shifted and non-shifted translation products share the same amino acid sequences in their N-terminal polypeptides coded by the 0 frame. By contrast, amino acid compositions coded by sequences downstream of the slippery site differ between the shifted and non-shifted products. Therefore, the effect of a new function gained from -1 PRF is determined by the frameshifting efficiency. Although the frameshifting efficiency is largely dependent on the potency of a stimulator, it is also affected by other parameters such as the spacer length and proximal sequence identity upstream of a slippery sequence (14,15). A viral protein capable of binding with signals downstream of a slippery sequence has been reported to stimulate -1 PRF (16,17), suggesting that trans-acting factors can be used to regulate the -1 PRF efficiency.

Studies attempting to exploit -1 PRF as a regulatory posttranscriptional gene expression circuit have reported that several RNA pseudoknots found in bacterial riboswitches can act as a ligand-dependent -1 PRF stimulator upon binding with their native ligands (18,19). However, because these pseudoknot-responsive ligands are cell metabolites, their applicability is limited. Alternatively, RNA pseudoknots capable of responding to non-metabolite small molecules for -1 PRF stimulation in trans have been generated through rational design or an in vitro selection process with limited success (20–22). However, both approaches can be time consuming. A simple and straightforward approach that uses ligands targeting the guanine to guanine (GG) mismatch within a duplex to stimulate -1 PRF was reported (23). This approach was based on the sensitivity of -1 PRF activity to the stability of the ribosome unwinding-resistant stem of a -1 PRF stimulator (24). Rationally designed and synthesized naphthyridine carbamate dimer (NCD) derivatives can act as a guanine-targeting ligand because they possess hydrogen bond-forming functional groups mimicking those observed in the Watson–Crick face of a cytidine base (25). The tetramer generated using two linked NCDs (NCT n , ' n ' represents the number of methylene units in the spacer) can target a GG mismatch within a 5'-CGG-3'/3'-GGC-5' motif. The binding mode of NCT n with the motif-inserted duplex might result from the formation of four GC pairing mimics between NCT n and the four guanines in the motif while repelling the two cytidine bases into solution. This mode is similar to that of naphthyridine-azaquinolone (NA) binding to the AA mismatch within a DNA duplex (26,27). Nuclear magnetic resonance (NMR) analysis of an NCD-bound 5'-GGA-3'/3'-AGG-5' GG-mismatch RNA motif consistently indicated the formation of two bulged adenines upon the formation of four GC pair mimics between two NCDs and this motif (28). Thus, the replacement of base pairs in the first stem (stem1) of a -1 PRF pseudoknot

with a 5'-CGG-3'/3'-GGC-5' motif can reduce -1 PRF activity because of the destabilization of stem1. However, -1 PRF stimulation can be restored upon the addition of the GG mismatch-targeting ligands because of the compensation for stability by the four GC base-pair mimics formed within the ligand–RNA complex. However, the GG mismatch motif-mediated stem destabilization still led to substantial residual -1 PRF activity that impaired the dynamic range of ligand-dependent -1 PRF stimulation. All of these approaches lacked the required efficient -1 PRF activity for practical application in regulating the cellular factors of mammalian cells that are tightly controlled in physiological conditions such as those in unfolded protein response (UPR).

A UPR is triggered by proteostasis imbalance in the endoplasmic reticulum (ER) when unfolded protein accumulation occurs in the ER (ER stress). The pathway is mediated by three ER-resident sensor proteins, PERK, IRE1 and ATF6 responsible for the activation of three downstream signaling cascades (29). Both PERK and IRE1 arms reduce the protein production load, with PERK acting as an attenuator of translation initiation and IRE1 controlling the decay of mRNA as well as the cytoplasmic splicing of the XBP-1 transcription activator mRNA. By contrast, the ER membrane-anchored ATF6 increases the protein-folding capacity through the ER stress-activated Golgi translocation of ATF6. The subsequent posttranslational cleavage releases a part of itself (ATF6N) to enter the cellular nucleus for the transcriptional activation of folding-related genes (30). Selective activation of the ATF6 axis without ER stress can be beneficial for the tailored production of specific secretory proteins because prolonged ER stress can harm cells, whereas the activation of the other two ER-stress branches tends to reduce the protein load. However, the specific transcriptional activation of isolated ATF6N to a physiologically relevant level has been difficult (31).

To overcome the bottleneck of ligand-dependent -1 PRF stimulator development, a straightforward approach without state-of-art selection or rational design for a specific ligand-stimulator pair is crucial. In this regard, the mismatch insertion approach might enable the creation of orthogonal -1 PRF stimulators responsive to distinct ligands by the swapping of different mismatch motifs. Such a plug-in strategy will benefit from a common stimulator scaffold possessing both a high frameshifting efficiency and reasonable dynamic range. A proof-of-principle study demonstrated that engineered mouse mammary tumor virus -1 PRF pseudoknot (MMTV-PK) mutants harboring a 5'-CGG-3'/3'-GGC-5' motif at stem1 responded to NCT n with frameshifting efficiencies of 1.5%–3% and a narrow dynamic range (23). We used a -1 PRF stimulator requiring stem-to-loop tertiary interactions for potent frameshifting activity as an engineering template to create an efficient and dynamic NCT n -dependent -1 PRF riboswitch. Subsequently, we used the optimized -1 PRF module to construct an RNA circuit to generate the ATF6N mimic through -1 PRF-mediated premature translation termination activated by GG mismatch-targeting ligands in the absence of an ER stress-inducing agent. The robust scaffold

established in this study can facilitate the creation of efficient orthogonal –1 PRF stimulators consisting of various mismatches that can be regulated by their targeting ligands for numerous applications in synthetic biology.

MATERIALS AND METHODS

Plasmid construction and mutagenesis

Standard cloning procedures were used to construct reporters, and the resultant recombinant vectors were transformed into the DH5 α strain of *Escherichia coli* cells for maintenance and selection by antibiotics. Mutagenesis was performed using the quick-change mutagenesis kit from Stratagene according to the manufacturer's instructions. Four sets of vectors were used in this study, and their constructions are described briefly below. The –1 PRF reporter plasmids were prepared through the following steps: amplified DNA fragments encoding mCherry were cloned into the EcoRI and Sall sites of super-fold GFP (sfGFP)-N1 (Addgene #54737) (32) to generate a dual-fluorescent reporter; nucleotide fragments containing the slippery sequence, spacer, and designed NCT7-responsive elements were generated through overlap extension polymerase chain reaction (PCR) as described previously (33); and purified blunt-ended fragments were digested using Sall and BamHI and then inserted between the Sall and BamHI sites of the dual-fluorescent reporter or p2luc vector (34). The M1 construct was generated by cloning the M1-VPK containing –1 PRF signal (23) into p2Luc. The in-line probing assay constructs were developed through the following steps: DNA fragments containing the T7 RNA polymerase promoter, sequences of the pseudoknot derivatives of interest, and the sequences of BbsI sites were generated using appropriate forward and reverse primers (Supplementary Table 1) through overlap extension PCR.

The DNA fragments obtained from overlap extension PCR were digested using HindIII and EcoRI restriction enzymes, and were cloned into PUC18 vectors to create pUC18-D1, pUC18-D4, pUC18-D5 and pUC18-DU177 as the templates for *in vitro* transcription. ATF6 related expression vectors were developed through the following steps: The pEGFP-ATF6-S1P was obtained by site-directed mutagenesis (R415A/R416A) using pEGFP-ATF6 (Addgene #32955) as the template (30). By contrast, DNA sequence of full-length ATF6 (amino acids 1–670) was amplified from pEGFP-ATF6 and cloned into the mammalian expression vector pFLAG-CMV2 to generate pFLAG-ATF6. The pFLAG-ATF6(2A) (F62A/L64A), pFLAG-ATF6-S1P (R415A/R416A) and pFLAG-ATF6(2A)-S1P were generated by PCR based site-directed mutagenesis using pFLAG-ATF6 as the template. The restriction sequences of *Sall* and *PstI* sites were then inserted between the coding sequences of amino acids 373 and 374 of ATF6 in pEGFP-ATF6-S1P, pFLAG-ATF6-S1P and pFLAG-ATF6(2A)-S1P by site-directed mutagenesis. Finally, the nucleotide fragments of D58 -1 PRF module were cloned between *Sall* and *PstI* sites of these three plasmids to form pEGFP-ATF6-S1P-FS, pFLAG-ATF6-S1P-FS and pFLAG-ATF6(2A)-S1P-FS, respectively. Plasmids for establishment of stable cell lines were generated through the following steps: The PB-T-PAF, PB-RN and the helper

plasmid PBCy43 that expresses PB transposase were gifts from Prof. J.M. Rini at the University of Toronto, Canada (35). The plasmid PB-T-Flag-ATF6-S1P-FS used for stable cell-line construction was generated by inserting the Flag-ATF6-S1P-FS fragment into the NheI and NotI sites downstream of the tetracycline responsive element (TRE) promoter of transposon-based PB-T-PAF vector. The luciferase gene of p5xATF6GL3 (Addgene #11976) (36) containing five repeats of ATF6 consensus DNA binding sites was replaced by mCherry ORF to generate the p5xATF6-mcherry reporter construct. The five ATF6 binding sites fused mCherry fragment of p5xATF6-mcherry was then cloned between BamHI and NotI sites of PB-RN to substitute for sequences of the CMV-rtTA region in PB-RN to generate PB-P5xATF6-mCherry.

In vitro and *in vivo* –1 PRF assays

In vitro –1 PRF assay was performed as described below: Capped reporter mRNAs were prepared by *in vitro* transcription. The *in vitro* transcription reaction mixtures containing NotI-digested p2luc-based reporter plasmid, methylated cap analogue (Epicentre) and T7 RNA polymerase were incubated at 37°C for 2 h. After adding DNaseI (RNase-free) (Ambion) to digest reporter plasmid, the capped reporter mRNAs were precipitated with ethanol and then recovered. The capped reporter mRNAs and Rabbit Reticulocyte Lysate, Nuclease-Treated (Promega) were used to generate *in vitro* translation protein products. The reaction was modified as followed: 100 ng capped reporter mRNA, 2.7 μ l rabbit reticulocyte lysate, 0.1 μ l amino acid mixture minus methionine, 0.1 μ l of RNase inhibitor (40 U/ μ l), 0.1 μ l of 10 μ Ci/ μ l [³⁵S]-labeled methionine (NEN) and 1 μ l of NCT-ligands of varied concentrations were mixed in a final 5 μ l of *in vitro* translation reaction. The reaction mixtures were incubated at 30°C for 2 h before loading into 12% SDS-PAGE. The dried gels were exposed using Typhoon FLA 7000 phosphorimager (GE) to measure the radioactivity of separated translation products. Frameshifting activity was calculated through dividing radioactive intensity of full-length shifted protein product by the sum of radioactive intensity of shifted and non-shifted protein products with the calibration of the methionine content of each protein as described before (20). We presented the effect of ligand on radioactivity-based -1 PRF activity in terms of relative –1 PRF activity by assuming similar extent of ribosome drop-off tendency during translation elongation (34) with or without ligand binding. Dual luciferase assay in cells was performed through the following steps: HeLa cells or HEK293T cells were cultured in Dulbecco's modified Eagle's medium (DMEM) (Gibco) supplemented with 10% fetal bovine serum (FBS) (Gibco), and grown in 24-well plate (0.5×10^5 or 1×10^5 cells per well). After growth at 37°C for 16–18 h, the cells were transfected with the mixture of 500 ng plasmid and FuGENE[®] HD Transfection Reagent (Promega) according to manufacturer's instructions and incubated for 24 h. The transiently transfected cells were distributed into 96-well plate (2×10^4 cells per well) and cultured for 24 h. The cells were treated with NCT7, Z-NCTS or NCD and then incubated for 24 h. Dual luciferase assays were performed using

the Dual-Glo[®] Luciferase Assay System (Promega). The procedure followed manufacturer's instructions with modification as below: after removing the medium, each well was added with 10 μ l 1 \times PBS and then mixed with 10 μ l Dual-Glo[®] Luciferase Reagent. The 96-well plate was incubated for 10 min at room temperature before detected by a Victor3 multi-label counter (PerkinElmer). Dual-luciferase based frameshifting efficiency of a specific construct was calculated as (Fluc/Rluc)/(Flucol/Rlucol) \times 100% according to previously described procedures by comparison with p2luci (34) or individual in-frame control construct as a control.

RNA preparation

The pUC18-D1, pUC18-D4, pUC18-D5 and pUC18-DU177 plasmids were linearized by BbsI digestion and used as templates to synthesize DU177-PK and engineered pseudoknot RNAs using T7 RNA polymerase. The GGA1 RNA was transcribed by T7 RNA polymerase using annealed top strand (5'-TAA TAC GAC TCA CTA TA-3') and template strand (5'-GTA CTT CCA CAT GAA ACA TGT TCC AGT ACC TAT AGT GAG TCG TAT TA-3') oligonucleotides that can hybridize to form T7 RNA polymerase promoter upstream of the DNA template (37). The RNA was purified from 15% denaturing polyacrylamide gel (29:1 acryl:bisacryl ratio) containing 8 M urea in the 1 \times TBE (Tris-borate-EDTA) buffer. The separated RNAs of interested were recovered from the gel and ethanol precipitated.

Non-denaturing gel-electrophoresis and In-line probing assay

The un-labelled RNAs were treated with calf intestine alkaline phosphatase (Roche), inactivated by heating and followed by the addition of T4 polynucleotide kinase (NEB) in the presence of [γ -³²P] ATP sequentially. The 5'-³²P-labelled RNAs were then purified and recovered by procedures described above. The non-denaturing gel-electrophoresis was performed as described below. The 5'-³²P-labelled D5-PK RNAs were heated at 95°C for 5 min and then were incubated with the NCT7 in 50 mM Tris-HCl pH 7.5, 50 mM NaCl and 10% glycerol at room temperature for 30 min. The mixtures were loaded into 10% (19:1) native polyacrylamide gels in 0.5X TBE buffer and were run for 10 min at 100 V and 35 min at 250 V at 4°C.

In-line probing assays were performed as described (22). In brief, the ³²P-labeled RNAs were incubated with or without GG-mismatch targeting ligands in in-line probing reaction buffer (50 mM Tris-HCl, pH8.3, 20 mM MgCl₂, 100 mM KCl) at 25°C for 40 h after boiling at 95°C for 2 min. The RNA ladders were generated by partially digestion of each labeled RNA through incubation in Alkaline Hydrolysis Buffer (Ambion) or with RNase T1 (Ambion) in 1 \times RNA Sequencing Buffer (Ambion). All reactions were terminated by adding gel loading buffer (95% formamide, 18 mM EDTA, 0.025% SDS, 0.025% xylene cyanol, 0.025% Bromophenol Blue) and then separated by 12% denaturing polyacrylamide gel (19:1 acryl:bisacryl ratio) in the 1 \times TBE buffer. The dried gels were exposed on a Typhoon FLA 7000 phosphorimager (GE).

Western blotting

HEK293T cells (1 \times 10⁵ per well) in 0.5 ml DMEM were grown in a 24-well plate for 16–18 h. After adding transfection mixture for 6 h, the medium was changed with DMEM containing 0.1 μ M NCT7 or 0.3 μ M Z-NCTS and incubated for 18 h. For the detection of EGFP-fused or FLAG-tagged ATF6, the cells were treated by 10 μ M MG-132 for 4 hr to block proteolytic activity before lysing the cell. The cells were lysed with RIPA lysis buffer (50 mM Tris-HCl, pH 7.5, 150 mM NaCl, 1 mM EDTA, 1% Triton X-100, 0.5% sodium deoxycholate, 0.1% SDS, cOmplete Protease Inhibitor Cocktail (Roche)) on ice for 10 min before 10 s sonication. The lysed cells were mixed with SDS sample loading buffer before loading into 8% SDS-PAGE and then analyzed by immunoblotting. By contrast, the protein products of fluorescence reporter were detected by procedure below: the transfected cells treated with NCT7 or Z-NCTS for 24 h were lysed with 60 μ l IP lysis buffer (50 mM HEPES-pH 7.5, 100 mM NaCl, 1 mM EDTA, 0.5% Triton X-100, 10% glycerol), and centrifuged to recover cell lysates. The supernatants were mixed with SDS sample loading buffer before loaded into 8% SDS-PAGE electrophoresis for separation. The gel with separated proteins was then transferred to a PVDF membrane (PerkinElmer) by a Trans-Blot semidry blotting system (Bio-Rad). After blocking treatment, the membrane was treated with the primary antibody mouse anti-FLAG (monoclonal antibody, 1:3000; SIGMA), mouse anti-mCherry (monoclonal antibody, 1:3000; Taiclone), chicken anti-GFP (polyclonal antibody, 1:3000; abcam) or mouse anti β -actin (monoclonal antibody, 1:5000; Proteintech), and followed by incubation with HRP-conjugated secondary antibody (anti-chicken IgG, 1:5000; Jackson or anti-mouse IgG, 1:5000; Jackson). The blot was then visualized by the addition of Western lighting plus ECL (PerkinElmer) and detected by a LAS-3000 luminescent image analyzer (FUJIFILM).

Fluorescent image analysis of fluorescent protein expression and Immunofluorescence

HEK293T cells were transfected onto coverslips in 24-well plate with 500 ng of pFLAG-ATF6(2A)-S1P-FS. The cells were incubated for 6 h and then treated with 0.1 μ M NCT7 for 24 h. After washing once with 1 \times PBS for 5 min, the cells were fixed in 4% paraformaldehyde for 10 min at room temperature, washed twice with 1 \times PBS for 5 min, and blocked with blocking buffer (0.1% Triton X-100 and 1% bovine serum albumin in PBS) for 30 min at room temperature. The cells were treated with anti-FLAG (1:250) monoclonal antibody in blocking buffer for 1 h at room temperature. The cells were then washed three times with 1 \times PBS for 5 min before incubating with Goat anti-Mouse IgG (H + L) Highly Cross-Adsorbed Secondary Antibody (Alexa Fluor Plus 488 conjugated) (Invitrogen) (1:500) in blocking buffer for 1 h at room temperature. After washing three times with 1 \times PBS for 5 min, the coverslips were mounted on microscope slides. The fluorescence images were observed by an epifluorescence microscope (Olympus BX51) and recorded with an Olympus DP71 camera system or by a confocal laser scanning microscopy (FV 3000, Olympus) using a 100 \times oil immersion objective lens with 405 and 488 nm laser

excitation. Transmitted light images were used for monitoring cell morphologies.

Stable cell line construction

Stable cell lines were established using a PiggyBac transposon system by the procedure described before (22,35). After growth in 24-well plate at 80% confluent, HEK293T cells were transfected with 400 ng PBT-Flag-ATF6-S1P-FS, 50 ng PB-RN and 50 ng PBCy43, and then selected by 250 μ g/ml G418 and 5 μ g/ml puromycin. After selection, surviving cells were treated with 4 μ g/ml tetracycline for 24 h and the expression of Flag-ATF6 was examined by immunofluorescence. This stable cell line was named HEK293T-FS1. By contrast, HeLa cells were first transfected with mixed plasmid DNA (450 ng PB-p5 xATF6-mcherry and 50 ng PBCy43), and selected by culturing in DMEM containing G418 (250 μ g/ml) for 2 weeks. The mCherry expression was confirmed by fluorescent microscope after adding 2 μ g/ml Tunicamycin (Tm) for 24 h. The mCherry positive cells were then co-transfected with 400 ng PBT-Flag-ATF6-S1P-FS, 50 ng PB-RN and 50 ng PBCy43, selected and examined as above. The resultant stable cell line was named HeLa-FS1.

Quantitative RT-PCR

HeLa-FS1 and HEK293T-FS1 cells were treated at 37°C with 4 μ g/ml tetracycline and 0.1 μ M NCT7 or 0.3 μ M Z-NCTS for 24 h or with 10 μ g/ml Tunicamycin (Tm) for 6 h. After purifying total cellular RNA by using the GENEzol™ TriRNA Pure Kit (Geneaid), the first strand cDNA was prepared from 1 μ g of total cellular RNA using the SuperScript™ III First-Strand Synthesis SuperMix for qRT-PCR (Invitrogen) following manufacturer's instructions. The cDNA, KAPA SYBR® FAST Universal Kit (Roche) and 0.15 μ M forward and reverse primers (Supplementary Table 2) (31) were used for amplification (6 min at 95°C then 45 cycles of 10 s at 95°C, 30 s at 60°C) in a Bio-RAD CFX96 Real Time PCR system. Gene expression values for all ATF6 and XBP1 targeted genes were normalized to the expression value of reference gene *Gapdh* before further analysis (31).

Statistical analysis of experimental data

Experiments were performed at least in triplicate unless indicated, and the relative frameshifting activity was reported as one standard deviation from the mean. The statistical significance was analyzed by two-tailed Student's *t*-test comparing between two groups and performed with SigmaPlot 12.5.

RESULTS

Identification of an efficient NCT7-dependent –1 PRF stimulator

Because the small size of MMTV-PK hindered further engineering, we looked for a potent –1 PRF pseudoknot stimulator with structure information and more engineering margins as the template for improvement. The DU177

pseudoknot (DU177-PK; Figure 1A) derived from the human telomerase RNA component (38) is a potent –1 PRF stimulator and thus a promising candidate (39,40). In addition to the hairpin-type pseudoknot topology, DU177-PK possesses extra base triples and cooperative tertiary stem1-to-loop2 interactions (Figure 1A) that contribute to its high activity (39–41). We speculated that inserting a 5'CGG3'/3'GGC5' motif in the stem1 of DU177-PK can interfere with the formation of tertiary networks required for high –1 PRF activity in addition to the stem destabilization that weakens ribosome-unwinding resistance. A combination of both effects can further reduce basal –1 PRF activity, thus increasing the dynamic range of ligand-dependent –1 PRF activation. Therefore, this artificial –1 PRF stimulator can be an ideal template to examine the potential of the mismatch insertion approach for creating efficient ligand-responsive –1 PRF stimulators.

The same strategy used in engineering MMTV-PK mutants (M1-VPK and M2-VPK) (23) was adopted for design. This strategy involved inserting a 5'CGG3'/3'GGC5' GG mismatch motif into DU177-PK stem1 and disrupting the terminal base pair of the stem to reduce stem stability (Figure 1A). However, residual frameshifting activity could still be high and compromise the dynamic range of ligand-induced –1 PRF as before. Unpublished works have indicated that the –1 PRF efficiency of DU177-PK is sensitive to stem2 integrity. Thus, we designed three DU177-PK mutants with distinct mismatch motif insertion patterns in stems to investigate the effect on residual –1 PRF activity reduction. The mismatch motif was inserted into the terminal end of DU177-PK stem2 (D1-PK) or DU177-PK stem1 (D2-PK) to prevent interference with the formation of base triples in the mutants, and D3-PK possessed two such motifs, with one in each stem (Figures 1A and 2A).

Each of the designed pseudoknots with an upstream UU-UAAAC slippery sequence and a spacer was cloned into a dual-luciferase –1 PRF reporter, p2Luc (34) to generate D1–D3 constructs for the in vitro translation assay. The –1 PRF signal was placed between the coding sequences of *Renilla* and firefly luciferase, with the firefly luciferase being placed in the –1 reading frame (Figure 1B). Therefore, the translation of firefly luciferase was used to monitor the occurrence of –1 frameshifting. NCT7 (Figure 1C) was used as the GG mismatch–targeting ligand for its higher binding affinity than that of other NCT derivatives (42). A comparison of the –1 PRF activity of the D1–D3 constructs before and after NCT7 treatment indicated a slight enhancement in –1 PRF activity in the presence of NCT7 for the D1 and D2 constructs (Figure 2B and C). The results also indicated that the basal –1 PRF activity of D2 was low, suggesting that the stem destabilization effect was achieved. By contrast, a synergistic –1 PRF activity enhancement was observed in the NCT7-treated D3 construct, implicating interaction between D3-PK and NCT7, although inefficient –1 PRF activity was observed in the presence of NCT7. On the basis of the binding model of the NCT7-bound 5'CGG3'/3'GGC5' motif, four GC-pairing mimics were formed within the complex (Supplementary Figure S1). Therefore, an extra base pair could form in the stem1 of NCT7-bound D2- and D3-PK compared with the stem1

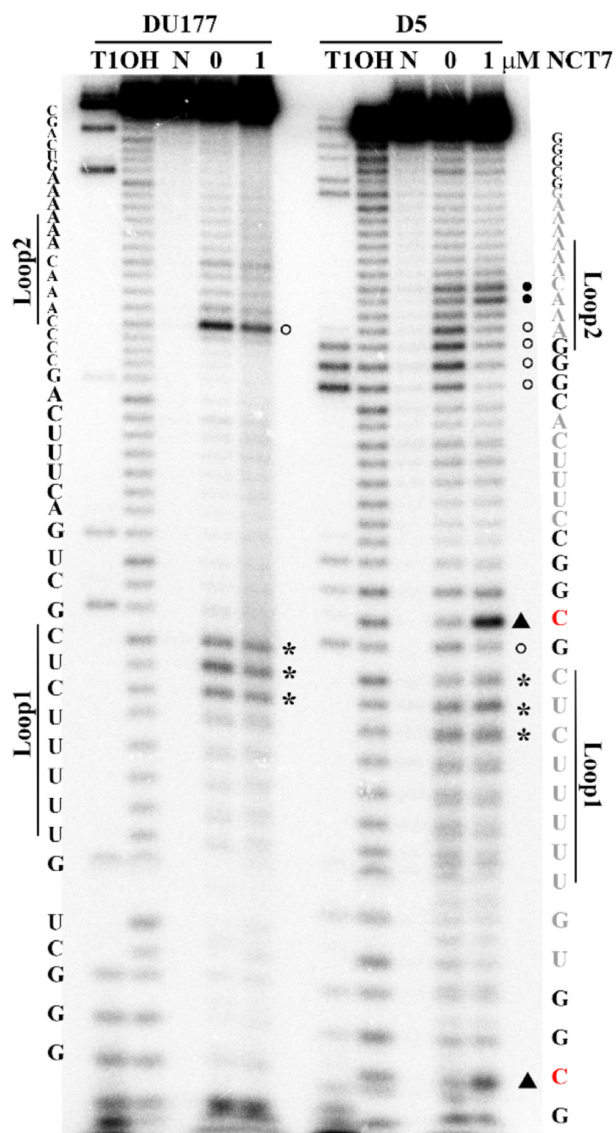


Figure 3. Spontaneous RNA hydrolysis analyses reveal NCT7 dependent conformational changes in 5'CGG3'/3'GGC5' GG-mismatch motifs of D5 pseudoknot. 12% denaturing gel analyses of in-line probing results of DU177-PK and D5-PK. Labels on the top of lanes in the gel image are experimental conditions described as the following: T1, partial digestion with RNase T1 (cleaves after G residues); OH, partial digestion with alkaline (cleaves at each internucleotide linkage); N, no reaction; 0, without NCT7; and 1, 1 μM NCT7. The assigned sequences for DU177-PK and D5-PK were based on the guanine-specific T1 ribonuclease cleavages, and are listed in the left and right of the image, respectively. * represents the flexible CUC sequences in the loop1 of each pseudoknot. An open circle represents reduced cleavage upon NCT7 treatment, whereas a dot represents enhanced cleavage upon NCT7 treatment. Triangle symbols indicate the enhanced internucleotide cleavages corresponding to the bulged-out cytosines (typed in red) in NCT7-bound 5'CGG3'/3'GGC5' GG mismatch motifs.

flanking cytosines (C26/C42). Although enhanced cleavages in C2 and C16 are consistent with higher flexibility caused by bulge formation upon NCT7 binding, the in-line probing results indicated that only one cytidine bulged out in each NCT7-bound mismatch motif within the complex. To further clarify these observations, the in-line probing

analyses of D1-PK and D4-PK under different NCT7 concentrations were performed; the results were compared with that of D5-PK (Supplementary Figures S4A–C). The D1-PK possessed identical stem2 sequence to that of D5-PK. A comparison of the in-line probing results of ligand-treated D1-PK and D5-PK revealed a similar NCT7-induced cleavage pattern variation in the 5'-side sequences of the inserted motif within each stem2. In particular, enhanced cleavage in the mismatch-flanking cytosine corresponding to the C16 in the stem2 of D5-PK was also observed in D1-PK. The D4-PK possessed identical stem1 sequence to that of D5-PK. A comparison of the in-line probing results of NCT7-treated D4-PK with those of D5-PK revealed a similar NCT7-induced cleavage pattern variation within the sequences of the inserted motif in each stem1. Furthermore, a marked cleavage reduction in the GGA sequences spanning stem1 to loop2 and a cleavage enhancement in the first mismatch-flanking cytosine (C2) that appeared in the stem1 of D5-PK were observed in D4-PK, too. Thus, NCT7 interacted with the inserted mismatch motifs within these engineered DU177-PK mutants.

To determine whether the difference between the results of in-line probing and those of the NMR structure model was due to the limitation of in-line probing, we performed in-line probing on a derivative of SCA31-HP RNA (GGA1) with or without NCD treatment. The NMR analysis of the NCD-bound SCA31-HP RNA possessing a 5'-GGA-3'/3'-AGG-5' GG mismatch motif in the middle of the hairpin stem indicated the formation of two bulges (28). The probing results revealed decreased cleavages in the four guanosines and increased cleavages in A9 and A25 of GGA1 RNA upon NCD treatment; the level of enhancement was higher for A25 than for A9 (Supplementary Figure S5A and B). This result indicated that in-line probing could detect the formation of GC pairing mimics and bulges in NCD-bound SCA31-HP RNA observed through NMR. Thus, the NCT7 binding modes of 5'-CGG-3'/3'-GGC-5' motifs within D5-PK could differ from those in a normal DNA or RNA duplex on the basis of the in-line probing results of the three analyzed DU177-PK mutants. However, the results of in-line probing analysis and dose-dependent –1 PRF activation by NCT7 (Supplementary Figure S2) indicated that the NCT7-mediated conformational rearrangement in D5-PK was directly related to the observed NCT7-dependent –1 PRF stimulation, suggesting that D5-PK is a –1 PRF riboswitch stimulator. Together with the compact RNA–ligand complexes observed through non-denaturing gel-electrophoresis, these results indicated that the observed –1 PRF activation by NCT7 was caused by the stabilized D5-PK RNA through interaction with the inserted mismatch motifs.

Optimization of NCT-dependent –1 PRF riboswitch activity in mammalian cells and ligand expansion

In addition to a stimulator, the slippery sequence, spacer length and proximal sequence identity upstream of the slippery sequence can affect –1 PRF efficiency (10,14,15). Therefore, we adjusted these parameters in the D5 construct to determine whether the ligand-dependent activation efficiency and dynamic range of –1 PRF could be im-

proved. Changing the slippery sequence to UUUUUUA or AAAAAC and the upstream E-site sequence to CGC or UCC did not increase but rather decreased the NCT7 dependent -1 PRF activity (data not shown). However, decreasing the spacer length from 6 to 5 (D58 construct) increased the -1 PRF efficiency by almost two folds, with a compromised dynamic range in the HEK293T cells (Supplementary Figure S6A and B). In vitro -1 PRF analyses of D5 and D58 constructs revealed a similar range of improvement in -1 PRF efficiency with reduced dynamic range for the D58 construct (Supplementary Figure S6C and D). To expand the range of cellular applications, the D5 and D58 constructs were investigated in different cell lines by using two other GG mismatch-targeting NCT analogs, namely NCD and Z-NCTS (44–46) (Supplementary Figure S6E and F). However, the performance of NCD was poorer than that of NCT7 in both constructs (Supplementary Figure S5B). By contrast, the level of -1 PRF stimulated by $0.3 \mu\text{M}$ Z-NCTS (with low toxicity) (47) for the D58 construct was similar to that stimulated by $0.1 \mu\text{M}$ NCT7 in both HeLa and HEK293T cells (Figure 4 A), thus providing an alternative for ligand selection.

Spacer length adjustment resulted in a difference in the amino acid composition encoded by a downstream pseudoknot because of changes in the reading frame. Because the amino acid composition encoded by the pseudoknot could affect the folding and activity of its nearby luciferases (48), the frameshifting efficiency calculation based on the measurement of fused luciferase activity could be inaccurate due to the interference of luciferase activity. To clarify this concern, an in-frame control for the D58 construct was generated for measuring the -1 PRF efficiency *in vivo*. The in-frame control construction involved disrupting the slippery sequence consensus and inserting an extra nucleotide in the spacer to reframe downstream sequences to the -1 frame. This led to the translation of a fusion protein mimicking the -1 PRF product without the occurrence of -1 PRF. Such a control can calibrate the potential interfering effect of the pseudoknot-encoded amino acid composition during the *in vivo* -1 PRF efficiency calculation (34). The *in vivo* -1 PRF efficiency of the D58 construct measured against the in-frame control (Supplementary Figure S6G) remained similar to that measured against the p2luci control (34) in Supplementary Figure S6B. Finally, the *in vivo* -1 PRF efficiency of M1-VPK (23) was measured using its own in-frame control (Supplementary Figures S6H) and compared with that of the D58 construct. Highly improved -1 PRF efficiency as well as dynamic range was achieved in the D58 construct.

The extension of the -1 frame C-terminal polypeptide is most frequently adopted in -1 PRF-mediated cellular activity in eukaryotic cells (19–22). To evaluate the application of an NCT-dependent -1 PRF stimulator in the extension mode, two fluorescent proteins were used to generate a -1 PRF reporter for the cellular imaging observation of NCT-dependent -1 PRF activity. To this end, a -1 PRF signal embedded with a 0 frame stop codon was inserted between the coding sequences of mCherry and sfGFP arranged in the 0 frame and -1 frame, respectively (Figure 1B). Without -1 PRF, the translation terminated before sfGFP, whereas sfGFP formation required the occur-

rence of -1 PRF. Therefore, NCT7-induced -1 PRF could be monitored on the basis of sfGFP fluorescent activity in cells transfected with this reporter. The -1 PRF signal of the D58 construct was used in the extension mode dual-fluorescent reporter because of its efficient -1 PRF efficiency measured in HEK293T and HeLa cells (Figure 4A). The -1 PRF signal of the D58 construct successfully induced sfGFP expression upon NCT7 or Z-NCTS treatment in HEK293T cells, as demonstrated by cell fluorescent imaging and the Western blotting of the cell lysate of reporter-transfected cells (Figures 4B, C). Thus, the -1 PRF signal of the D58 construct could efficiently respond to NCT ligands in the extension mode in different human cell lines. Together, these findings indicated that the use of DU177-PK as the engineering template substantially improved NCT-dependent -1 PRF activity, thus making the application of ligand-dependent -1 PRF for mediating mammalian cellular functions more realistic.

Premature translational termination as a regulatory gene expression mode in mammalian cells

Premature translation termination mediated by -1 PRF is frequently observed in prokaryotic systems (49–52). However, the adoption of this functional mode in mammalian cells has not been established. We explored the possibility of applying the D58 module to build a circuit capable of triggering premature translation termination to overcome the restriction imposed on other mammalian cellular pathways not involving -1 PRF. The ER membrane-bound ATF6 consists of an N-terminal bZIP domain, a transmembrane domain, and a C-terminal luminal domain. Unfolded protein accumulation in the ER triggers the delivery of ATF6 to the Golgi for sequential cleavages (first in the S1P site and then in the S2P site) by Golgi-resident proteases (31) (Figure 5A). Such cleavages cause the release of the N-terminal bZIP to enter the nucleus and activate specific UPR genes for the expansion of the protein-folding capacity in the ER. We speculated that the protease cleavage-dependent release of ATF6N could be mimicked by -1 PRF-mediated premature translation termination to sidestep the ER stress requirement. This means that a -1 PRF-mediated circuit could be built to boost the ER protein-folding capacity in an ER-stress independent manner.

To this end, an EGFP-fused ATF6 (a wild-type construct) was mutated at the first protease cleavage site (S1P) that traps the mutant (the S1P construct) in the Golgi under ER stress conditions (Supplementary Figure S7A). A designed D58 module capable of inducing premature translation termination upon NCT7 treatment was inserted before the protease cleavage sites in the transmembrane domain of the S1P construct (the FS construct). With this design, ligand treatment resulted in translation termination before the ribosome reached the membrane domain, thus mimicked physiological ATF6N released during ER stress. Western blotting analysis of the cell lysates of 293T cells transfected by these constructs was performed. The results revealed a low-molecular weight product, presumably EGFP-ATF6N, in the WT construct treated with MG132, a proteasome inhibitor, and an ER stress-inducing reagent (53). By contrast, little EGFP-ATF6N was observed in the S1P

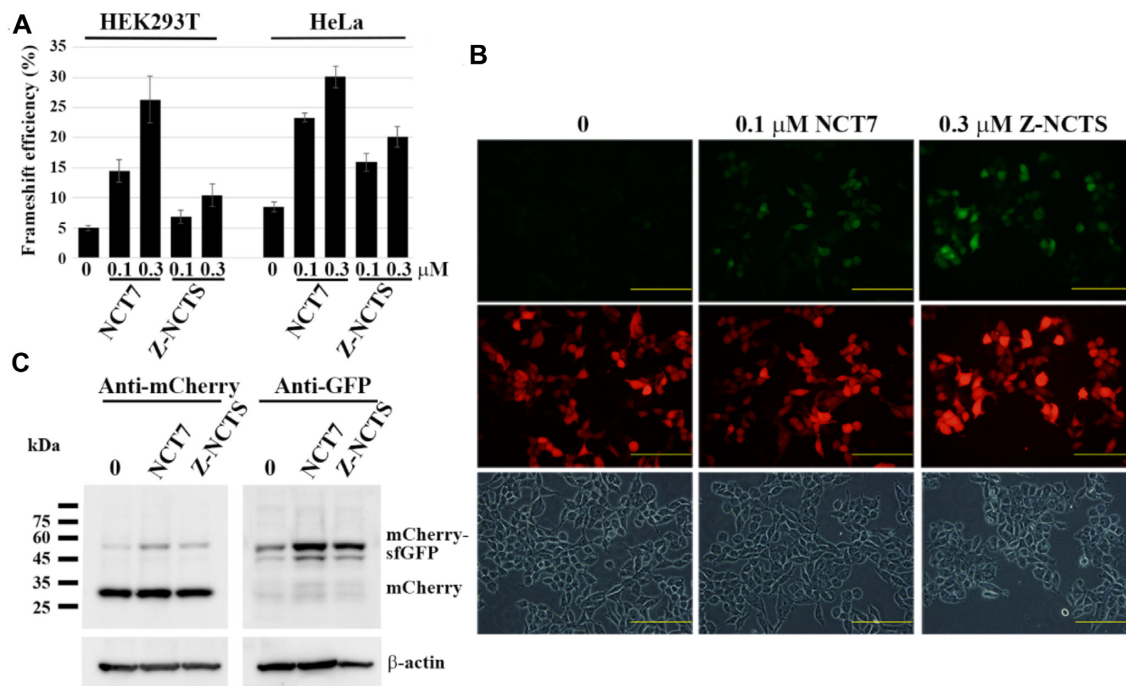


Figure 4. Comparisons of NCT ligands-dependent -1 PRF activity of D58 construct in different human cell-lines. (A) The -1 PRF efficiency of D58 construct with different NCT ligands in different cell-types calculated from dual-luciferase assay results using its own in-frame control. Value for each bar is the mean of six independent experiments with standard deviation of the mean. (B) Fluorescent imaging analyses of HEK293T cells transfected by the D58 -1 PRF signal-containing dual-fluorescent reporter with or without ligand induction. The signals shown in the three horizontal rows were from the detection of: top panel, sfGFP (-1 frame); middle panel, mCherry (0 frame); bottom panel, bright field. (C) Results of Western-blot analysis of the cell lysates of dual-fluorescent reporter transfected cells in (B) using anti-mCherry (in 0 frame) or anti-GFP (in -1 frame) antibody. The cell lysates were collected after the treatment of NCT ligands for 24 h.

construct treated with MG132 in addition to the full-length product, indicating that the S1P construct was resistant to the ER stress-mediated protease cleavage. The appearance of the EGFP-ATF6N mimic was prominent only when the FS construct was treated with NCT7 or Z-NCTS (Supplementary Figure S7B); these results are consistent with the occurrence of ligand-dependent -1 PRF-mediated premature translation termination. Therefore, this proof-of-principle pilot study demonstrated that -1 PRF-mediated premature translation termination was functional in a mammalian cell.

Non-ER stress-mediated ATF6 activation by a ligand-dependent -1 PRF circuit

Because the fused EGFP of EGFP-ATF6N could hinder entry into the nucleus, a set of new constructs was prepared by replacing fused EGFP with a FLAG tag for further analysis of the ATF6N mimic generation (Figure 5B). A readthrough control (the RT construct) that could generate FLAG-ATF6N as the main product was designed as a positive control. No FLAG-ATF6N was detected in the Western blotting analysis when the anti-FLAG antibody was used (data not shown). One study reported that the released ATF6N is unstable and can be stabilized with mutations in two residues (F62/L64) within ATF6N; however, such mutations can attenuate transcriptional activation (54). To ensure the formation of -1 PRF-mediated ATF6N mimics, F62A/L64A mutations were introduced into all FLAG-

tagged, ATF6-related constructs (with 2A designation). With such modifications, the Western blotting analysis of the cell lysates of HEK293T cells transfected with these FLAG-tagged 2A expression constructs was performed again. The results (Figure 5C) indicated that ATF6(2A)-S1P-FS-transfected cells possessed very low level of premature translation termination product in relative to cells transfected with the readthrough control (RT). However, treatment with NCT7 or Z-NCTS enhanced the level of the premature translation termination product, indicating activated -1 PRF activity by the ligand-dependent -1 PRF circuit. The nucleus localization of released FLAG-ATF6N(2A) was examined by comparing the immunofluorescent imaging of the FS construct-transfected HEK293T cells with or without NCT7 treatment with a confocal microscope (Figure 5D). By contrast with the evenly distributed FLAG-ATF6N(2A) within the nucleus, the signal of FLAG-ATF6(2A) was mainly localized in the cytoplasm in cells without NCT7 treatment. Therefore, the ATF6N mimic generated by ligand-dependent -1 PRF-mediated premature termination was capable of entering the nucleus. Next, a tetracycline-inducible 293T stable cell-line (HEK293T-FS1) harboring the FLAG-ATF6-S1P-FS construct (without 2A mutation to prevent transcription activity attenuation) was established. HEK293T-FS1 was examined for ATF6N mimic expression through Western blotting in the presence of both tetracycline and NCT. The formation of -1 PRF-mediated ATF6N mimics upon tetracycline induction and either NCT7 or Z-NCTS treat-

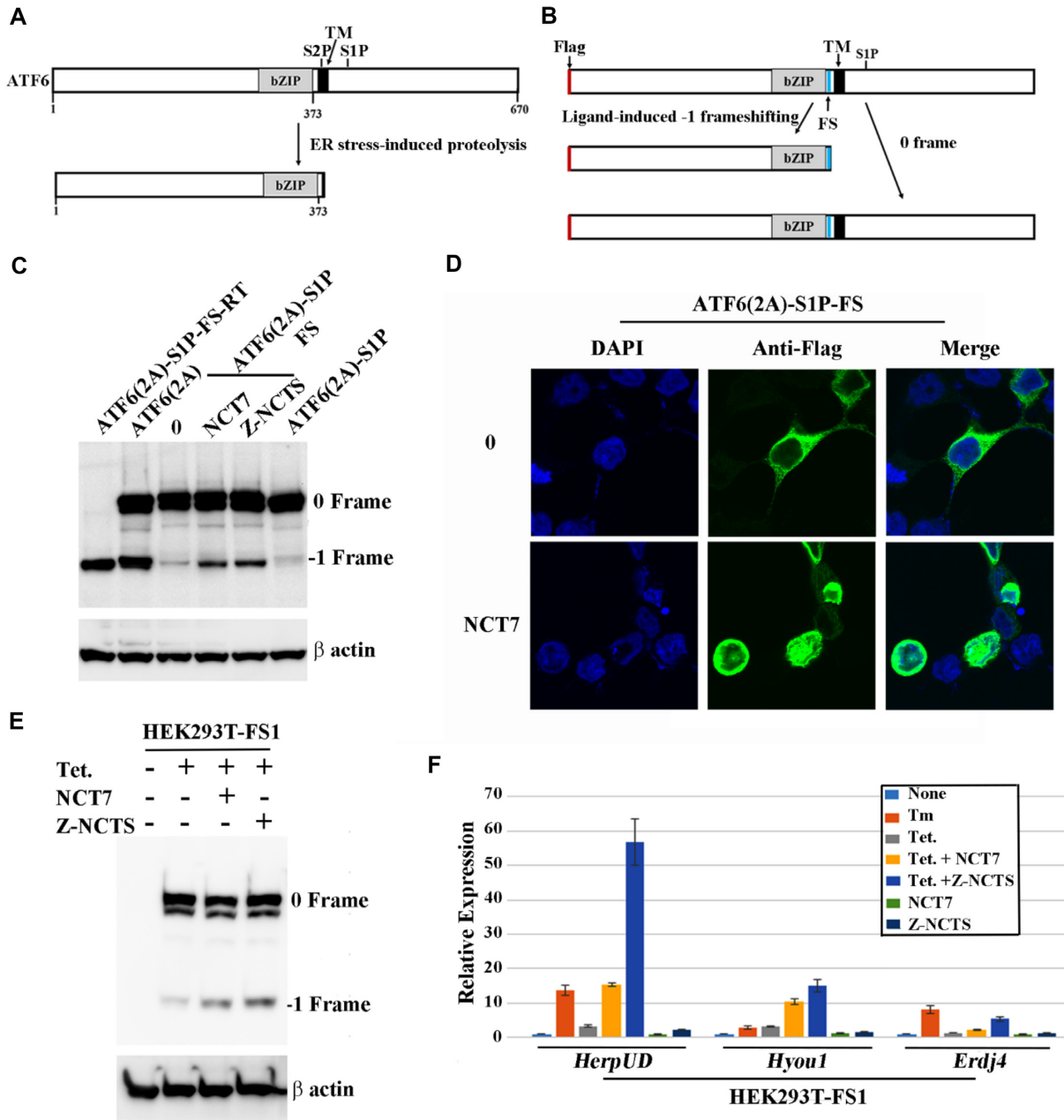


Figure 5. Functional ATF6N mimic formation by NCT-dependent -1 PRF mediated premature translation termination in human HEK293T cell-lines. (A) Diagram of ER stress-induced processing of ATF6. The positions of bZIP domain, transmembrane (TM) domain, S1P and S2P are indicated. (B) Scheme of FLAG-ATF6-SIP construct derived translation products by engineered NCT7-induced -1 PRF. The positions of FLAG-tag, bZIP domain, transmembrane (TM) domain and S1P cleavage site are also indicated. The -1 PRF signal (FS) capable of mediating NCT7-induced premature termination was inserted between amino acids 373 and 374 of ATF6 (in blue). The -1 frame and 0 frame translation products will lead to the synthesis of FLAG-tagged ATF6N mimic and full-length ATF6 chimera, respectively. (C) Western blot analyses of FLAG-ATF6N mimic formation in HEK293T cells transfected with FLAG-ATF6(2A) -SIP-FS related expression vectors. The cells transfected with plasmid (pFLAG-ATF6(2A)-SIP-FS), containing S1P (R415A/R416A) and -1 PRF signal were treated with NCT7 (0.1 μ M) or Z-NCTS (0.3 μ M). The proteins extracted from transfected cells were detected by anti-FLAG antibody. The pFLAG-ATF6(2A)-SIP-FS-RT is a readthrough construct serving as a positive control for FLAG-ATF6N mimic formation. (D) Immunofluorescence analyses of nucleus localizing FLAG-ATF6N mimic in transfected HEK293T cells by confocal microscope. Cells on slide glasses transfected with pFLAG-ATF6(2A)-SIP-FS were treated with NCT7 (0.1 μ M). The cells were fixed and stained with anti-FLAG antibody and secondary antibody conjugated Alexa Fluor® Plus 488 sequentially (right panel) and DAPI (left panel). Bar, 10 μ m. (E) Western blot analyses of NCT-induced FLAG tagged ATF6N mimics in a -1 PRF circuit harboring HEK293T-FS1 stable cell line. The expression of -1 PRF circuit was under the control of the tetracycline promoter P_{TRE} . The cell line was treated with tetracycline (4 μ g/ml) and NCT7 (0.1 μ M) or Z-NCTS (0.3 μ M) for 24 h. The proteins extracted from HEK293T-FS1 were detected with anti-FLAG antibody. (F) The qRT-PCR analyses of *HerpUD*, *Hyou1* and *Erdj4* in the HEK293T-FS1 in (E). The cell line was treated with tetracycline (4 μ g/ml) and NCT7 (0.1 μ M) or Z-NCTS (0.3 μ M) for 24 h or with 10 μ g/ml Tunicamycin (Tm) for 6 h. The qRT-PCR values are relative to the cell line without ligand treatment and the value for each bar is the mean with standard deviation of the mean.

ment could be observed without 2A mutation modification (Figure 5E). The expression pattern was similar to that of the transient expression of 2A modification (Figure 5C), although the expression level was lower in HEK293T-FS1 cells. ATF6N and XBP1 are basic leucine zipper transcription factors that can increase the expression of distinct but overlapping sets of genes. Therefore, real-time quantitative PCR (qRT-PCR) was performed using primers designed for specific ATF6 or XBP1 downstream genes (Supplementary Table 2) to examine the specificity of ATF6N mimic. Consistent with the entry of the ATF6N mimic into the nucleus, the results revealed the expression of the ATF6-specific *HerpUD* mRNA over the XBP1-specific *Erdj4* mRNA as well as *Hyou1* mRNA that was targeted by both ATF6 and XBP1 in the presence of tetracycline and either NCT ligand (Figure 5F). Thus, the premature termination-mediated mimic of the ATF6N polypeptide was functional within HEK293T cells.

To evaluate the transcriptional activity of the -1 PRF-generated FLAG-ATF6N mimic for its general application in different cell types, we constructed a fluorescent reporter encoding an mCherry gene driven by an upstream UPR promoter (UPR-mCherry). A HeLa stable cell line (HeLa-FS1) harboring the UPR-mCherry reporter as well as a tetracycline-inducible FLAG-ATF6-S1P-FS circuit was established. Treatment of HeLa-FS1 with tunicamycin (Tm), an ER stress-inducing drug, led to the expression of mCherry without the nucleus localization of the FLAG-ATF6N mimic; this finding is consistent with the activation of the UPR promoter-driven mCherry by Tm-mediated endogenous ER stress (Figure 6A). Treatment with tetracycline and either NCT7 or Z-NCTS led to the detection of the fluorescent imaging of both the UPR-mCherry and nucleus-localized FLAG-ATF6N mimic. This contrasts the cytoplasm retention of the full-length FLAG-ATF6-S1P-FS-encoded protein when only tetracycline was administered (Figure 6A). In addition, HeLa-FS1 was treated with NCT7 or Z-NCT alone without tetracycline, and the expression of neither UPR-mCherry nor FLAG-ATF6 was observed (Supplementary Figure S8). Thus, the observed ATF6N activation was not caused by NCT7 or Z-NCTS itself but by ligand-mediated -1 PRF. To examine the specificity of the -1 PRF-generated FLAG-ATF6N mimic, qRT-PCR was performed using primers designed for specific genes targeted by the different branches of UPR to compare relative mRNA expression levels under different conditions. Three ATF6-targeting genes (*Bip*, *HerpUD* and *Pdia4*), two XBP1-targeting genes (*Erdj4* and *Satt3a*), and one gene targeted by both (*Hyou1*) were examined (31). The results of qRT-PCR revealed that all three ATF6-specific genes could be activated by the ATF6N mimic, with *HerpUD* exhibiting the highest mRNA expression level, followed by *Bip*, *Pdia4*, and *Hyou1*. By contrast, the mRNA levels of XBP1-specific *Erdj4* and *Satt3a* were not affected by ATF6N mimic formation (Figure 6B). Therefore, the results indicated that the -1 PRF-mediated ATF6N mimic was both functional and specific, although the induced mRNA expression levels were weaker than those observed after Tm treatment (Figure 6C). Together, these results demonstrated that the -1 PRF-mediated RNA circuit could activate the functional ATF6N mimic without

the use of an ER-stress-inducing agent in both 293T and HeLa cells.

DISCUSSION

Based on the NCTn-dependent -1 PRF stimulation in engineered MMTV-PK mutants containing an inserted 5'-CGG-3'/3'-GGC-5' motif in stem1, we demonstrated that the same approach can be applied to a different pseudoknot with substantial improvement in both the dynamic range and efficiency of -1 PRF activity. This was achieved by selecting a potent -1 PRF stimulator, DU177-PK, that requires both stem integrity and stem-loop tertiary interactions to stimulate -1 PRF activity as the building template. With the insertion of the 5'-CGG-3'/3'-GGC-5' motif in the stems of such a template, the intricate tertiary interaction network between stem1 and loop2 could be disrupted in addition to the destabilization of the stem. Therefore, both the effects could suppress the -1 PRF efficiency synergistically, thus further reducing basal -1 PRF activity. By contrast, the restoration of stem1-loop2 interaction could be coupled to base pairing reformed in the stem upon interaction with the GG-mismatch targeting ligand to amplify the compensation effect of complex formation. However, the *in vitro* -1 PRF efficiency of NCT7-bound D5-PK was $<50\%$ that of DU177-PK, although the dynamic range was markedly improved (Figure 2 and Supplementary Figure S2). One possible reason is that the stem reformation mediated by ligand binding is not capable of fully restoring the stem1-loop2 interaction required for high -1 PRF efficiency considering that ligand binding might lead to the formation of bulge-out cytidine to interfere with proximal tertiary interactions. Consistently, although the change in the in-line cleavage pattern in D5-PK upon NCT7 treatment supported NCT7 binding and stem restoration, the enhanced cleavage in the AC step within the AAAC sequences in loop2 (Figure 3) suggested a more flexible conformation in both nucleotides within the complex compared with free D5-PK. By contrast, the same region of DU177-PK was less accessible to cleavage; this is consistent with the formation of tertiary stem1-loop2 interactions. Nevertheless, the performance of D5-PK was sufficient for the application purpose.

In studies examining the application of ligand-dependent -1 PRF activity, the C-terminal extension mode with fluorescent activity detection was usually used as the model (19–22) probably because the extended domain can provide a gain of function activity even when -1 PRF activity is low. The increase in -1 PRF efficiency to 25% observed in this study can help build an applicable ligand-dependent -1 PRF circuit for synthetic gene regulation in mammalian cells. The premature translation termination mode of -1 PRF was evaluated and applied successfully to a real mammalian cellular pathway in different cell types. Because premature termination-mediated regulatory gene expression is not observed in mammalian systems, it is ideal for synthetic purposes to regulate cellular processes involving the C-terminal domain function of a protein. In this study, it was used to mimic the protease cleavage-mediated release of ATF6N from the membrane-anchored domain of ATF6. We found that the ATF6N mimic was detected only in the presence of the

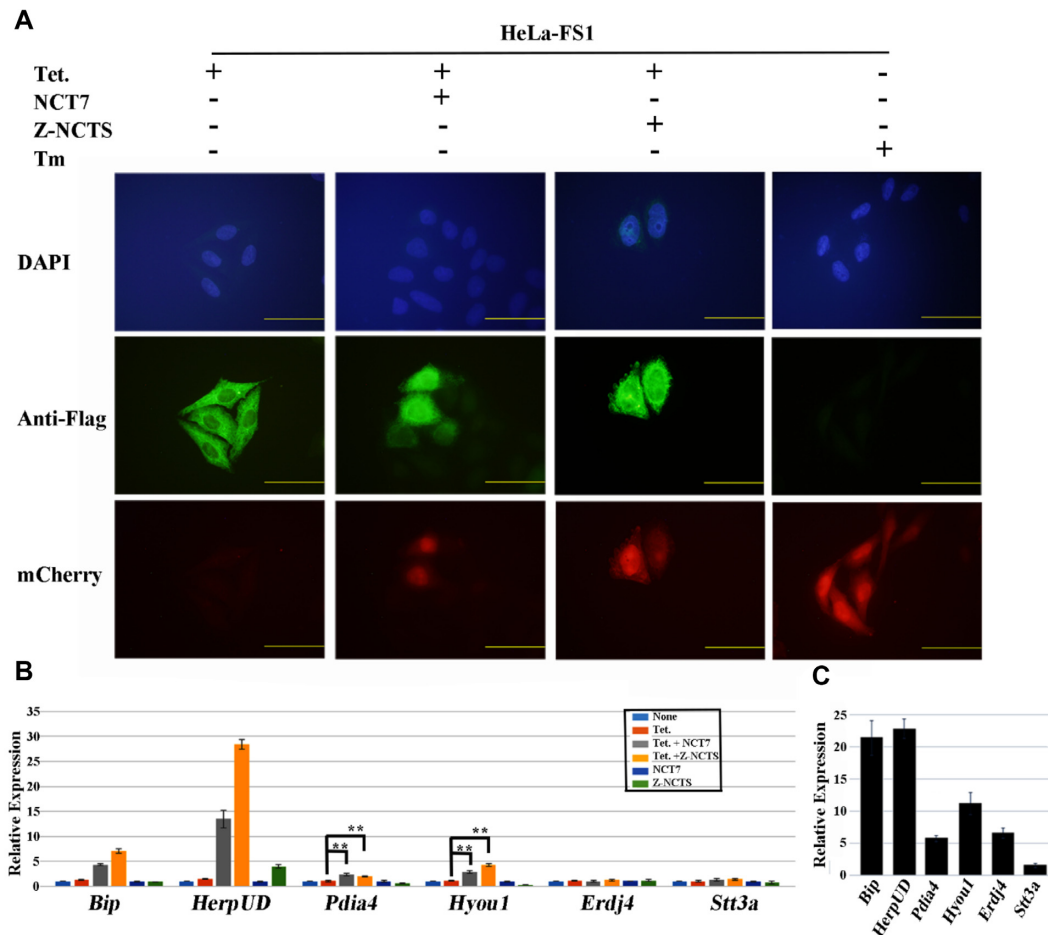


Figure 6. Activation of ATF6-specific gene expression by ATF6N mimic generated from NCT-dependent -1 PRF circuit in HeLa-FS1 stable cell line. (A) Fluorescence microscopy images of -1 PRF circuit mediated gene expression in HeLa-FS1. The cell line was treated with tetracycline ($4 \mu\text{g/ml}$) and NCT7 ($0.1 \mu\text{M}$) or Z-NCTS ($0.3 \mu\text{M}$) for 48 h or with $2 \mu\text{g/ml}$ Tm for 1 day. The cells were fixed and stained with DAPI (upper panel), anti-Flag antibody and secondary antibody conjugated Alexa Fluor[®] Plus 488 sequentially (middle panel). The images of ATF6N-induced mCherry were showed in lower panel. Bar, $10 \mu\text{m}$. (B) The qRT-PCR analyses of ATF6 and XBP1s target genes in the HeLa-FS1 in (A) following expression of -1 PRF circuit and treatment with NCT7 ($0.1 \mu\text{M}$) or Z-NCTS ($0.3 \mu\text{M}$) for 24 h. The qRT-PCR values are relative to the cell line without ligand treatment, and are presented as mean with standard deviation of the mean. ** means $P < 0.001$ as determined by student's t -test. (C) The qRT-PCR analyses of ATF6 and XBP1 targeting genes of HeLa-FS1 in (A) following treatment with $10 \mu\text{g/ml}$ Tm for 6 h. The relative expression levels are calculated by comparing with those without ligand treatment after normalization, and the value for each bar is the mean with standard deviation of the mean.

proteasome inhibitor MG132 in Western blotting analysis, indicating its existence is under stringent regulation. This result suggested that high -1 PRF efficiency is crucial for successful application in tightly regulated processes when the active form of a factor of interest must be rapidly inhibited within cells. The two modes of -1 PRF (premature termination and C-terminal extension) may have unique advantages in the toolbox of synthetic circuits to address problems involving the inclusion or exclusion of a C-terminal membrane-anchoring domain as well as an organelle-targeting signal.

The binding mode of NCTn with the $5'$ -CGG- $3'$ / $3'$ -GGC- $5'$ motif within D5-PK was assumed to be similar to those of the NMR-based structural models of complexes formed between NCD-derived ligands and a $5'$ -CGG- $3'$ / $3'$ -GGC- $5'$ or a $5'$ -GGA- $3'$ / $3'$ -AGG- $5'$ GG mismatch motif within a duplex (26–28). Although the in-line probing analysis of NCT7-bound D5-PK in this study provided confor-

mational rearrangement information in the NCT7–D5PK complex, only enhanced cleavages corresponding to the first guanosine-paired cytosine flanking the GG mismatch in $5'$ -CGG- $3'$ / $3'$ -GGC- $5'$ motif was observed in each stem. By contrast, in-line cleavage patterns corresponding to the counterpart cytosines were not enhanced by NCT7 treatment, suggesting a low-flexibility environment for these two cytosines (Figure 3). Such differences could result from the base-triple interaction network within the pseudoknot topology of D5-PK because the NMR analysis of ligand-bound GG-mismatch motifs was performed within a normal duplex context. Therefore, the exact binding mode of the GG-mismatch targeting ligand within D5-PK should be characterized through a high-resolution structural analysis with NMR or X-ray crystallography.

We noticed stimulated *HerpUD* expression by Z-NCTS alone from the qRT-PCR results in HeLa-FS1 (Figure 6B), whereas no similar stimulation was observed in other genes

or in HEK293T-FS1 (Figure 5F). However, the successful adoption of Z-NCTS in D58 construct stimulation (Figure 4) indicates that a similar binding mode could be conserved in this class of GG mismatch–targeting ligands, thus warranting modification to reduce the cellular toxicity of the ligand and achieve further improvement. Several other ds-DNA mismatch (AA/CC)–targeting ligands are available and could be converted to an RNA mismatch–targeting ligand with modification (25,55). Within this context, the D5-PK established in this study can be used as the scaffold with plug-in potential by different mismatch compositions to generate a versatile platform for building orthogonal ligand–specific –1 PRF stimulators. Such a platform can help promote the development of other synthetic mismatch–targeting ligands by using rational design.

DATA AVAILABILITY

Raw data are available from the corresponding author upon request.

SUPPLEMENTARY DATA

Supplementary Data are available at NAR Online.

ACKNOWLEDGEMENTS

We thank Mr. Che-Pei Cho for management of the lab and reading of the manuscript. This manuscript was edited by Wallace Academic Editing.

FUNDING

Ministry of Science and Technology (MOST) of Taiwan [105-2311-B-005-004-MY3 and 109-2311-B-005-010]. Funding for open access charge: MOST [110-2311-B-005-010].

Conflict of interest statement. None declared.

REFERENCES

- Way, J.C., Collins, J.J., Keasling, J.D. and Silver, P.A. (2014) Integrating biological redesign: where synthetic biology came from and where it needs to go. *Cell*, **157**, 151–161.
- Nissim, L., Wu, M.R., Pery, E., Binder-Nissim, A., Suzuki, H.I., Stupp, D., Wehrspau, C., Tabach, Y., Sharp, P.A. and Lu, T.K. (2017) Synthetic RNA-based immunomodulatory gene circuits for cancer immunotherapy. *Cell*, **171**, 1138–1150.
- Wong, R.S., Chen, Y.Y. and Smolke, C.D. (2018) Regulation of t cell proliferation with drug-responsive microRNA switches. *Nucleic Acids Res.*, **46**, 1541–1552.
- Isaacs, F.J., Dwyer, D.J. and Collins, J.J. (2006) RNA synthetic biology. *Nat. Biotechnol.*, **24**, 545–554.
- McKeague, M., Wong, R.S. and Smolke, C.D. (2016) Opportunities in the design and application of RNA for gene expression control. *Nucleic Acids Res.*, **44**, 2987–2999.
- Etzel, M. and Mörl, M. (2017) Synthetic riboswitches: from plug and pray toward plug and play. *Biochemistry*, **56**, 1181–1198.
- Yokobayashi, Y. (2019) Aptamer-based and aptazyme-based riboswitches in mammalian cells. *Curr. Opin. Chem. Biol.*, **52**, 72–78.
- Farabaugh, P.J. (1996) Programmed translational frameshifting. *Annu. Rev. Genet.*, **30**, 507–528.
- Atkins, J.F., Loughran, G., Bhatt, P.R., Firth, A.E. and Baranov, P.V. (2016) Ribosomal frameshifting and transcriptional slippage: from genetic steganography and cryptography to adventitious use. *Nucleic Acids Res.*, **44**, 7007–7078.
- Brierley, I., Jenner, A.J. and Inglis, S.C. (1992) Mutational analysis of the “slippery-sequence” component of a coronavirus ribosomal frameshifting signal. *J. Mol. Biol.*, **227**, 463–479.
- Giedroc, D.P. and Cornish, P.V. (2009) Frameshifting RNA pseudoknots: structure and mechanism. *Virus Res.*, **139**, 193–208.
- Tu, C., Tzeng, T.H. and Bruenn, J.A. (1992) Ribosomal movement impeded at a pseudoknot required for frameshifting. *Proc. Natl Acad. Sci. U.S.A.*, **89**, 8636–8640.
- Takyar, S., Hickerson, R.P. and Noller, H.F. (2005) mRNA helicase activity of the ribosome. *Cell*, **120**, 49–58.
- Kim, Y.G., Maas, S. and Rich, A. (2001) Comparative mutational analysis of cis-acting RNA signals for translational frameshifting in HIV-1 and HTLV-2. *Nucleic Acids Res.*, **29**, 1125–1131.
- Léger, M., Dulude, D., Steinberg, S.V. and Brakier-Gingras, L. (2007) The three transfer RNAs occupying the a, p and e sites on the ribosome are involved in viral programmed -1 ribosomal frameshift. *Nucleic Acids Res.*, **35**, 5581–5592.
- Li, Y., Treffers, E.E., Naphthine, S., Tas, A., Zhu, L., Sun, Z., Bell, S., Mark, B.L., van Veelen, P.A., van Hemert, M.J. et al. (2014) Transactivation of programmed ribosomal frameshifting by a viral protein. *Proc. Natl. Acad. Sci. U.S.A.*, **111**, E2172–E2181.
- Naphthine, S., Ling, R., Finch, L.K., Jones, J.D., Bell, S., Brierley, I. and Firth, A.E. (2017) Protein-directed ribosomal frameshifting temporally regulates gene expression. *Nat. Commun.*, **8**, 15582.
- Chou, M.Y., Lin, S.C. and Chang, K.Y. (2010) Stimulation of -1 programmed ribosomal frameshifting by a metabolite-responsive RNA pseudoknot. *RNA*, **16**, 1236–1244.
- Yu, C.H., Luo, J., Iwata-Reuyl, D. and Olsthoorn, R.C. (2013) Exploiting preQ1 riboswitches to regulate ribosomal frameshifting. *ACS Chem. Biol.*, **8**, 733–740.
- Hsu, H.T., Lin, Y.H. and Chang, K.Y. (2014) Synergetic regulation of translational reading-frame switch by ligand-responsive RNAs in mammalian cells. *Nucleic Acids Res.*, **42**, 14070–14082.
- Anzalone, A.V., Lin, A.J., Zairis, S., Rabadan, R. and Cornish, V.W. (2016) Reprogramming eukaryotic translation with ligand-responsive synthetic RNA switches. *Nat. Methods*, **13**, 453–458.
- Lin, Y.H. and Chang, K.Y. (2016) Rational design of a synthetic mammalian riboswitch as a ligand-responsive -1 ribosomal frame-shifting stimulator. *Nucleic Acids Res.*, **44**, 9005–9015.
- Matsumoto, S., Caliskan, N., Rodnina, M.V., Murata, A. and Nakatani, K. (2018) Small synthetic molecule-stabilized RNA pseudoknot as an activator for -1 ribosomal frameshifting. *Nucleic Acids Res.*, **46**, 8079–8089.
- Garcia-Miranda, P., Becker, J.T., Benner, B.E., Blume, A., Sherer, N.M. and Butcher, S.E. (2016) Stability of HIV frameshift site RNA correlates with frameshift efficiency and decreased virus infectivity. *J. Virol.*, **90**, 6906–6917.
- Nakatani, K. (2009) Recognition of mismatched base pairs in DNA. *Bull. Chem. Soc. Jpn.*, **82**, 1055–1089.
- Peng, T. and Nakatani, K. (2005) Binding of naphthyridine carbamate dimer to the (CGG)_n repeat results in the disruption of the G-C base pairing. *Angew. Chem. Int. Ed. Engl.*, **44**, 7280–7283.
- Nakatani, K., Hagihara, S., Goto, Y., Kobori, A., Hagihara, M., Hayashi, G., Kyo, M., Nomura, M., Mishima, M. and Kojima, C. (2005) Small-molecule ligand induces nucleotide flipping in (CAG)_n trinucleotide repeats. *Nat. Chem. Biol.*, **1**, 39–43.
- Shibata, T., Nagano, K., Ueyama, M., Ninomiya, K., Hirose, T., Nagai, Y., Ishikawa, K., Kawai, G. and Nakatani, K. (2021) Small molecule targeting r(UGGAA)_n disrupts RNA foci and alleviates disease phenotype in *Drosophila* model. *Nat. Commun.*, **12**, 236.
- Walter, P. and Ron, D. (2011) The unfolded protein response: from stress pathway to homeostatic regulation. *Science*, **334**, 1081–1086.
- Chen, X., Shen, J. and Prywes, R. (2002) The luminal domain of ATF6 senses endoplasmic reticulum (ER) stress and causes translocation of ATF6 from the ER to the golgi. *J. Biol. Chem.*, **277**, 13045–13052.
- Shoulders, M.D., Ryno, L.M., Genereux, J.C., Moresco, J.J., Tu, P.G., Wu, C., Yates, J.R. 3rd, Su, A.I., Kelly, J.W. and Wiseman, R.L. (2013) Stress-independent activation of XBP1s and/or ATF6 reveals three functionally diverse ER proteostasis environments. *Cell Rep.*, **3**, 1279–1292.
- Pédélec, J.D., Cabantous, S., Tran, T., Terwilliger, T.C. and Waldo, G.S. (2006) Engineering and characterization of a superfolder green fluorescent protein. *Nat. Biotechnol.*, **24**, 79–88.

33. Casimiro, D.R., Toy-Palmer, A., Blake, R.C. II and Dyson, H.J. (1995) Gene synthesis, high-level expression, and mutagenesis of thiobacillus ferrooxidans rusticyanin: his 85 is a ligand to the blue copper center. *Biochemistry*, **34**, 6640–6648.
34. Grentzmann, G., Ingram, J.A., Kelly, P.J., Gesteland, R.F. and Atkins, J.F. (1998) A dual-luciferase reporter system for studying recoding signals. *RNA*, **4**, 479–486.
35. Li, Z., Michael, I.P., Zhou, D., Nagy, A. and Rini, J.M. (2013) Simple piggyBac transposon-based mammalian cell expression system for inducible protein production. *Proc. Natl. Acad. Sci. U.S.A.*, **110**, 5004–5009.
36. Wang, Y., Shen, J., Arenzana, N., Tirasophon, W., Kaufman, R.J. and Prywes, R. (2000) Activation of ATF6 and an ATF6 DNA binding site by the endoplasmic reticulum stress response. *J. Biol. Chem.*, **275**, 27013–27020.
37. Milligan, J.F. and Uhlenbeck, O.C. (1989) Synthesis of small RNAs using T7 RNA polymerase. *Methods Enzymol.*, **180**, 51–62.
38. Theimer, C.A., Blois, C.A. and Feigon, J. (2005) Structure of the human telomerase RNA pseudoknot reveals conserved tertiary interactions essential for function. *Mol. Cell*, **17**, 671–682.
39. Chen, G., Chang, K.Y., Chou, M.Y., Bustamante, C. and Tinoco, I. Jr (2009) Triplex structures in an RNA pseudoknot enhance mechanical stability and increase efficiency of -1 ribosomal frameshifting. *Proc. Natl. Acad. Sci. U.S.A.*, **106**, 12706–12711.
40. Chou, M.Y. and Chang, K.Y. (2010) An intermolecular RNA triplex provides insight into structural determinants for the pseudoknot stimulator of -1 ribosomal frameshifting. *Nucleic Acids Res.*, **38**, 1676–1685.
41. Chen, Y.T., Chang, K.C., Hu, H.T., Chen, Y.L., Lin, Y.H., Hsu, C.F., Chang, C.F., Chang, K.Y. and Wen, J.D. (2017) Coordination among tertiary base pairs results in an efficient frameshift-stimulating RNA pseudoknot. *Nucleic Acids Res.*, **45**, 6011–6022.
42. Matsumoto, S., Hong, C., Otabe, T., Murata, A. and Nakatani, K. (2013) Ligand-inducible formation of RNA pseudoknot. *Bioorg. Med. Chem. Lett.*, **23**, 3539–3541.
43. Soukup, G.A. and Breaker, R.R. (1999) Relationship between internucleotide linkage geometry and the stability of RNA. *RNA*, **5**, 1308–1325.
44. Hong, C., Hagihara, M. and Nakatani, K. (2011) Ligand-assisted complex formation of two DNA hairpin loops. *Angew. Chem. Int. Ed. Engl.*, **50**, 4390–4393.
45. Hong, C., Otabe, T., Matsumoto, S., Dohno, C., Murata, A., Hagihara, M. and Nakatani, K. (2014) Formation of a ligand-assisted complex of two RNA hairpin loops. *Chem. Eur. J.*, **20**, 5282–5287.
46. Dohno, C., Kohyama, I., Kimura, M., Hagihara, M. and Nakatani, K. (2013) A synthetic riboswitch that operates using a rationally designed ligand-RNA pair. *Angew. Chem. Int. Ed.*, **52**, 9976–9979.
47. Dohno, C., Kimura, M. and Nakatani, K. (2018) Restoration of ribozyme tertiary contact and function by using a molecular glue for RNA. *Angew. Chem. Int. Ed. Engl.*, **57**, 506–510.
48. Loughran, G., Howard, M.T., Firth, A.E. and Atkins, J.F. (2017) Avoidance of reporter assay distortions from fused dual reporters. *RNA*, **23**, 1285–1289.
49. Blinkowa, A.L. and Walker, J.R. (1990) Programmed ribosomal frameshifting generates the escherichia coli DNA polymerase III γ subunit from within the τ subunit reading frame. *Nucleic Acids Res.*, **18**, 1725–1729.
50. Flower, A.M. and McHenry, C.S. (1990) The γ subunit of DNA polymerase III holoenzyme of escherichia coli is produced by ribosomal frameshifting. *Proc. Natl. Acad. Sci. U.S.A.*, **87**, 3713–3717.
51. Tsuchihashi, Z. and Kornberg, A. (1990) Translational frameshifting generates the gamma subunit of DNA polymerase III holoenzyme. *Proc. Natl. Acad. Sci. U.S.A.*, **87**, 2516–2520.
52. Meydan, S., Klepacki, D., Karthikeyan, S., Margus, T., Thomas, P., Jones, J.E., Khan, Y., Briggs, J., Dinman, J.D., Vázquez-Laslop, N. et al. (2017) Programmed ribosomal frameshifting generates a copper transporter and a copper chaperone from the same gene. *Mol. Cell*, **65**, 207–219.
53. Diakiw, S.M., Perugini, M., Kok, C.H., Engler, G.A., Cummings, N., To, L.B., Wei, A.H., Lewis, I.D., Brown, A.L. and D'Andrea, R.J. (2013) Methylation of KLF5 contributes to reduced expression in acute myeloid leukaemia and is associated with poor overall survival. *Br. J. Haematol.*, **161**, 884–888.
54. Thuerauf, D.J., Morrison, L.E., Hoover, H. and Glembotski, C.C. (2002) Coordination of ATF6-mediated transcription and ATF6 degradation by a domain that is shared with the viral transcription factor, VP16. *J. Biol. Chem.*, **277**, 20734–20739.
55. Mukherjee, S., Błaszczyk, L., Rypniewski, W., Falschlunger, C., Micura, R., Murata, A., Dohno, C., Nakatani, K. and Kiliszek, A. (2019) Structural insights into synthetic ligands targeting A-A pairs in disease-related CAG RNA repeats. *Nucleic Acids Res.*, **47**, 10906–10913.